JOURNAL OF THE ROYAL SOCIETY Interface

J. R. Soc. Interface (2011) **8**, 1155–1165
doi:10.1098/rsif.2010.0578
Published online 18 January 2011

Optimality of the Münch mechanism for translocation of sugars in plants

K. H. Jensen[1,†], J. Lee[2,†], T. Bohr[3], H. Bruus[1], N. M. Holbrook[4,*] and M. A. Zwieniecki[5]

[1]*Centre for Fluid Dynamics, Department of Micro- and Nanotechnology, Technical University of Denmark, DTU Nanotech Building 345 East, 2800 Kongens Lyngby, Denmark*
[2]*Division of Engineering, Brown University, Providence, RI 02912, USA*
[3]*Centre for Fluid Dynamics, Department of Physics, Technical University of Denmark, DTU Physics Building 309, 2800 Kongens Lyngby, Denmark*
[4]*Department of Organismic and Evolutionary Biology, and* [5]*Arnold Arboretum, Harvard University, Cambridge, MA 02138, USA*

Plants require effective vascular systems for the transport of water and dissolved molecules between distal regions. Their survival depends on the ability to transport sugars from the leaves where they are produced to sites of active growth; a flow driven, according to the Münch hypothesis, by osmotic gradients generated by differences in sugar concentration. The length scales over which sugars are produced (L_{leaf}) and over which they are transported (L_{stem}), as well as the radius r of the cylindrical phloem cells through which the transport takes place, vary among species over several orders of magnitude; a major unsettled question is whether the Münch transport mechanism is effective over this wide range of sizes. Optimization of translocation speed predicts a scaling relation between radius r and the characteristic lengths as $r \sim (L_{\mathrm{leaf}}\, L_{\mathrm{stem}})^{1/3}$. Direct measurements using novel *in vivo* techniques and biomimicking microfluidic devices support this scaling relation and provide the first quantitative support for a unified mechanism of sugar translocation in plants spanning several orders of magnitude in size. The existence of a general scaling law for phloem dimensions provides a new framework for investigating the physical principles governing the morphological diversity of plants.

Keywords: phloem transport; sugar translocation; microfluidics; biomimetics; osmotic pumping

1. INTRODUCTION

Vasculatures of plants and animals are among the most elegant and complex of microfluidic systems. In plants, xylem transports water from soil to leaves, while phloem distributes the products of photosynthesis throughout the plant. Flow generation in both systems occurs in the absence of any mechanical pump. Xylem flow is generated by evaporation and driven by tension gradient in the vessels [1]. The physics of transport under tension creates a safety–efficiency optimization problem that constrains the design of xylem vessels [2]. The mechanism driving phloem transport is believed to be the movement of water via osmosis in response to the loading and unloading of sugar in different parts of the plant and sustained along the tubes by continuous maintenance of the osmotic gradient across the perimeter of the phloem tube, as shown in figure 1 [3,4]. Phloem operates under positive pressure and the assumed mode of its generation results in the delivery of sugars being controlled by their loading and unloading rates [5,6], rather than by the velocity of the flow. However, phloem distributes hormonal and signalling molecules that allow for the integration of distal parts in lieu of a designated nervous system [7,8]. This additional signalling task could result in the selection pressure to optimize translocation velocity by providing plants with the ability to respond rapidly to environmental perturbations [9]. Here we ask if phloem is indeed optimized for speed. Further, we investigate if a single scaling law can describe the design principles of phloem tubes governing the speed of translocation given the wide range of length scales existing in nature. Phloem tube radii range from 1 to 40 μm, their length from 0.01 to 100 m, with transport velocities from 0.01 to 1 m h^{-1} [10–12].

Studies of long-distance transport in plants are inherently difficult because the fluxes are intracellular, protected by physical barriers [13] or biological activity (e.g. forisomes and p-proteins [14,15]), and occur under large tensions or pressures [16]. In principle, these properties require *in vivo* approaches, which are prone to methodological challenges. However, recent biomimetic approaches have helped answer long-standing questions regarding water transport in the xylem [17] and to resolve optimization laws governing the placement of

*Author for correspondence (holbrook@oeb.harvard.edu).
†These authors contributed equally to the study.

Received 20 October 2010
Accepted 21 December 2010

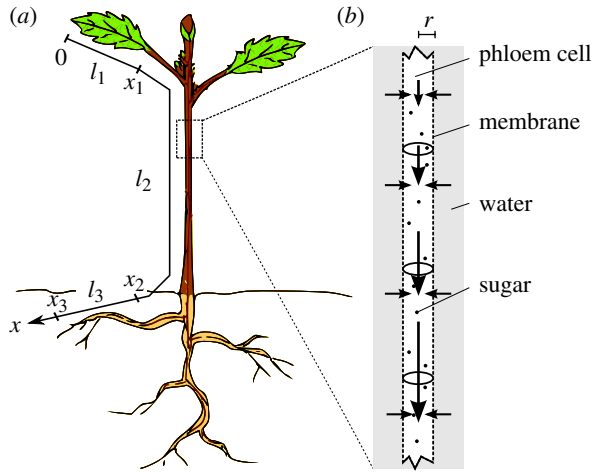

Figure 1. (*a*) Schematic of a plant in which sugar and signalling molecules travel from sources, e.g. leaves, to places of storage and growth, e.g. fruits or roots. In our model, the plant is divided into three zones, a source/loading zone of length l_1 (the leaf; $0 < x < x_1$), a translocation zone of length l_2 (the stem; $x_1 < x < x_2$) and a sink/unloading zone of length l_3 (the root; $x_2 < x < x_3$). (*b*) Diagram of how the Münch flow mechanism is thought to drive sugar translocation in plants. The surfaces of the cylindrical phloem cells of radius r are covered by a semi-permeable membrane. Sugar loaded actively into the cells at the sugar source draws water by osmosis from the surrounding tissue, thereby generating flow as the sugar solution is displaced downstream. (Online version in colour.)

veins within leaves [18], both processes being part of the transpiration stream [1]. Progress in the fabrication of microfluidic devices has made it possible to mimic phloem transport [19], providing a physical model to test Münch theory [20]. Here, we use synthetic phloem to resolve design properties underlying the delivery of photoassimilate and chemical signals between distal plant parts and to provide a mechanistic basis for the implementation of our mathematical model of phloem function.

Many of the published models of phloem transport incorporate details of sugar loading and unloading (e.g. [21–24]). In contrast, our goal was to study a simplified model, which agrees with the general trends previously reported, but which due to its simplicity lends itself to a scaling analysis. To determine if real plants follow the scaling relation predicted by our mathematical model, we examined phloem dimensions and transport velocities in real plants using a novel, non-invasive, dye-tracing method that offers a significant improvement to the previously used techniques such as traditional dye tracing [25], biomass accumulation [26] or tracing radioactive carbon [27], while accommodating a broader range of plant materials than magnetic resonance imaging [12]. We also compared published data on sieve tube radii with the optimal radii calculated from our model.

2. MATERIAL AND METHODS

To study osmotically driven flows in microchannels, we designed and fabricated a microfluidic system consisting of two layers of 1.5 mm thick polymethyl methacrylate (PMMA) separated by a semi-permeable membrane (Spectra/Por Biotech cellulose ester dialysis membrane, MWCO 3.5 kDa, thickness 40 μm), as shown in figure 2*a*. Channels of length 27 mm, width 200 μm and depth $h = 100–200$ μm were milled in the two PMMA layers using a MiniMill/Pro3 milling machine [19]. The top channel contains partly the sugar solution and partly pure water, while the bottom channel always contains only pure water. Inlets were produced by drilling 800 μm diameter holes through the wafer and inserting brass tubes into these. By removing the surrounding material, the channel walls in both the top and bottom layers acquired a height of 100 μm and a width of 150 μm. After assembly, the two PMMA layers were positioned such that the main channels in either layer were facing each other. Thus, when clamping the two layers together using four 10 mm paper clamps, the membrane acted as a seal, stopping any undesired leaks from the channels as long as the applied pressure did not exceed approximately 100 kPa.

The top channel was connected at one end to a syringe pump (NE-1000, New Era syringe pump, NY), which continuously injected a solution of water, dextran (17.5 kDa, Sigma-Aldrich) 1 μm polystyrene beads (Sigma-Aldrich, L9650-1ML, density 1050 kg m^{-3}) into the channel at flow velocities of 2–4 μm s^{-1}. At the other end, the channel was left open with the outlet terminating in an open reservoir. Both ends of the lower 'pure water' channel were connected to this reservoir to minimize the hydrostatic pressure difference across the membrane and to prevent axial flow in this channel. The flow velocity inside the upper channel was recorded by tracking the motion of the beads. Image sequences were recorded at different positions along the channel using a Unibrain Fire-i400 1394 digital camera attached to a Nikon Diaphot microscope with the focal plane at $h/2$ and a focal depth of approximately 10 μm. The flow behaved as if it were pressure-driven and the standard laminar flow profile was used to determine the average flow velocity [19].

To determine rates of phloem transport *in vivo*, an aqueous solution (100 mg l^{-1}) of 5(6)-carboxyfluorescein diacetate was placed onto gently abraded upper leaf epidermis from where it was loaded into the phloem by the plant (figure 2*b*) [28,29]. We tracked the dye, as it moved in the phloem of petioles or stems, by photobleaching flow velocity techniques that were previously used in microfluidic systems [30,31]. However, these single-detector techniques required modification to accommodate measurements on living plant tissues (low velocities, tissue light scattering and absorption, the need to maintain favourable growth conditions). We used two solid-state, high-gain photodiodes (SED033 used with IL1700 Research Radiometer, International Light Technologies) separated by a known distance to determine travel time of the photobleached pulse. The photodiodes were connected to the stem/petiole via bifurcated, 4 mm diameter optical fibres to obtain a sufficient signal-to-noise ratio despite extremely low light intensities. Excitation light was delivered via 490 nm short-pass filters (Omega Optical, USA), while photodiodes were fitted with 510 nm long-pass filters (Omega Optical). Excitation light was generated by narrow

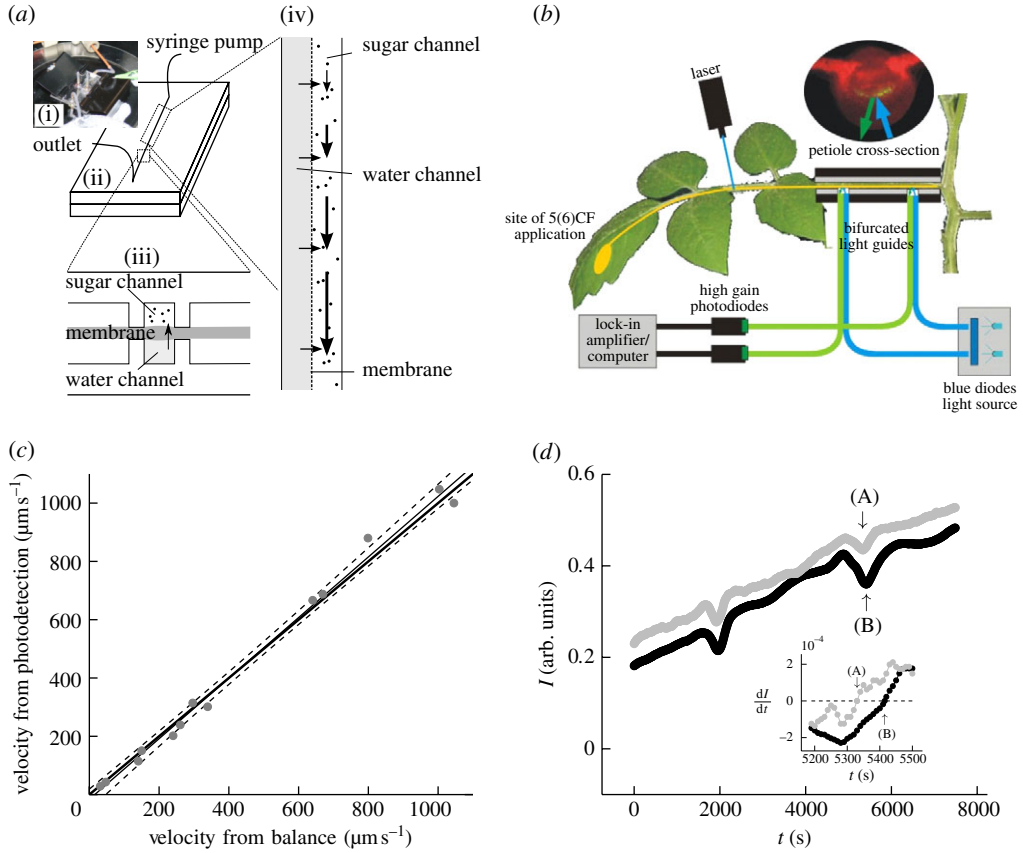

Figure 2. (*a*) Microfluidic set-up. (i) Picture of the microfluidic device used to biomimic the phloem transport system. (ii,iii) Schematic of the microfluidic device. Two microchannels are in osmotic contact through a semi-permeable membrane. One, the bottom channel, remains filled with pure water while the other contains a sugar solution injected slowly at one end by a syringe pump. (iv) Close-up showing the flow mechanism driving sugar translocation in the microfluidic system. (*b*) Sketch of the set-up used to determine phloem flow rate in tomato petioles. (*c*) Comparison of flow velocities in a 1.19 mm diameter glass capillary determined by our photobleaching technique and by a standard mass flow-rate technique (filled circles, measurements; thin line, regression; dashed line, 95% confidence interval; thick line, one to one relation). (*d*) Two consecutive measurements of the relative intensity I of the fluorescence versus time t detected by the two photodiodes shown in (*b*). The flow velocity u is determined by measuring the traversal time between the two diodes, marked by arrows (A,B), of a minimum in I induced by photobleaching of the dye using a short (less than 30 s) laser pulse. The inset shows $\partial I/\partial t$ versus time; the intensity minima (indicated by arrows (A,B)) are given by $\partial I/\partial t = 0$ (black circles, sensor 1; grey circles, sensor 2). (Online version in colour.)

band blue diodes (470 nm, Roithner LaserTechnik GmbH, Switzerland). Fibres were attached to the plant through custom-made, light-tight clips. A bleached pulse was produced ahead of the detection system by a 20 mW laser of wavelength 473 nm (Dragon Laser, China) as sketched in figure 2*b*. All filters and laser parameters were chosen to accommodate properties of the 5(6)-carboxyfluorescein diacetate dye.

The set-up was tested by comparing flow velocity determined by photodetection with values $u = Q/(2\pi r^2)$ obtained from volume flow rate Q as measured by a microbalance (Sartorius 210DX ± 0.01 mg) and the radius r of the capillary tube (figure 2*c*). We generated velocities from 20 to 1000 μm s^{-1}, similar to the measured *in vivo* phloem velocities. The signal output is Gaussian-shaped, figure 2*d*, due to the convolution of the 4 mm wide detection window (set by the optical fibre diameter) and the internal dispersion-widened bleaching pulse combined with light scattering in the plant tissues. Thus, the flow velocity u was determined by measuring the traversal time between the two diodes of a minimum intensity of fluorescence following the photobleaching of the dye using a 30 s laser pulse. The same procedure was used on the plants (figure 2*d*). We note that the technique is independent of dye loading rate and tissue light properties.

3. RESULTS

In plants, phloem transport initiates in the leaves, where sugar is actively loaded into sieve tubes, and ends in growth or storage zones, where sugar is unloaded. We may think of the plant aligned with x-axis as being divided into three zones: (i) a loading zone $(0 < x < x_1)$ of length $l_1 = x_1$ (essentially the length of the leaf); (ii) a translocation zone $(x_1 < x < x_2)$ of length $l_2 = x_2 - x_1$ (essentially the length the plant, typically much larger than l_1); and (iii) an unloading zone $(x_2 < x < x_3)$ of length $l_3 = x_3 - x_2$, where the sugar is consumed (figure 1; table 1). The flow rate through a phloem tube depends on the osmotic driving force, the radius r of the tube, its length l_2 and the effective viscosity η of the fluid including the effect of sieve plates [6,32]. The most important characteristic of this relation is that, fixing all other parameters,

Table 1. Nomenclature.

parameter	symbol	value and/or unit
length	x	m
viscosity	η	Pa s
membrane permeability	L_p	$\mathrm{m\,s^{-1}\,Pa^{-1}}$
length of leaf	l_1, L_leaf	m
length of stem	l_2, L_stem	m
length of root	l_3	m
radius of phloem tube	r	m
optimal radius	r_c	m
water flow through tube wall	J	$\mathrm{m\,s^{-1}}$
pressure	p	Pa
osmotic flow velocity scale	U	$\mathrm{m\,s^{-1}}$
Münch number	$M\ddot{u}$	dimensionless
leaf to stem length ratio	α	dimensionless
dimensionless sugar concentration gradient in root	β	dimensionless
volume flux	Q	$\mathrm{m^3\,s^{-1}}$
gas constant	R	$\mathrm{m^3\,Pa\,K^{-1}\,mol^{-1}}$
temperature	T	K
wall resistance	R_w	$\mathrm{Pa\,m^{-3}\,s}$
tube resistance	R_t	$\mathrm{Pa\,m^{-3}\,s}$
velocity	u	$\mathrm{m\,s^{-1}}$
dimensionless velocity	v	dimensionless
dimensionless length	ξ	dimensionless
dimensionless concentration	ς	dimensionless
height of channel	h	m
intensity of fluorescence	I	arb. units
time	t	s

it is non-monotonic in r giving maximal flow rate at a particular value denoted r_c. This is easily understood since the behaviour for large and small r is strongly dependent on the ratio of the resistance of the flow in the channel to the resistance (or the inverse of the permeability L_p) across the semi-permeable membrane, a non-dimensional quantity we call the Münch number $M\ddot{u}$ [33],

$$M\ddot{u} = 16\,\frac{\eta L_\mathrm{p} l_2^2}{r^3}. \tag{3.1}$$

For wide tubes ($M\ddot{u} \ll 1$) there is essentially no viscous pressure gradient along the tube, but the efficacy of the osmotic pump is small. On the other hand, for narrow tubes ($M\ddot{u} \gg 1$), where the osmotic driving force is strong, the viscous pressure gradient in the tube becomes important and the flow is impeded.

The water flow J across the membrane of the tube at position x is determined by the local difference $c(x)$ in sugar concentration and in pressure $p(x)$ across the membrane. In a tube at temperature T,

$$J(x) = L_\mathrm{p}[RTc(x) - p(x)] \tag{3.2a}$$

and together with conservation of fluid volume, this leads to the Münch equation for the gradient of the velocity $u(x)$ in the translocation zone

$$\frac{\partial u}{\partial x} = \frac{2L_\mathrm{p}}{r}\,(RTc - p), \quad \text{for } x_1 < x < x_2. \tag{3.2b}$$

Here, we assume ideality of the sugar solution, a semi-permeable membrane with unity reflection coefficient, and slow flow velocities relative to transverse diffusion such that radial gradients are weak. Also, we are assuming that the external pressure and concentration do not vary—aside from hydrostatic pressure differences owing to height variations. This is clearly a strong simplification since of course the phloem flow is not independent of the state of the xylem. However, all of our phloem flow measurements were conducted under low-light thus minimizing transpiration-induced gradients in xylem pressure [12]. The neglect of external variations in the sugar concentration is partly due to the way our model is formulated, since the strong variations in concentrations between leaf and root are modelled as *internal* variations in the tube.

The pressure gradient for such slow flows is given by the Hagen–Poiseuille–Darcy relation

$$\frac{\partial p}{\partial x} = -\left(\frac{8\eta}{r^2}\right) u \tag{3.2c}$$

valid even taking into account the radial, osmotic inflow [34,35]. We verified (figure 3*a*) the description (3.2*a*)–(3.2*c*) of osmotic transport by comparing measurements of osmotically driven flows through microfluidic channels (described in detail in [19]) with analytical solutions of the flow problem in the limit $M\ddot{u} \ll 1$ (see appendix A), under the boundary conditions of a fixed concentration and velocity at x_1 and a fixed pressure ($p = 0$) at x_2, boundary conditions used in previous experimental studies [36,37]. Fabrication of devices working in the limit $M\ddot{u} \gg 1$ is difficult owing to the properties of currently available artificial membranes, channel lengths and bonding burst pressures, and we have not been able to realize this limit.

To examine how velocity scales with the full range of radial and axial phloem dimensions found in plants we formulated a simple model (see appendix A for further details), which gives a complete overview of the concentration and velocity profiles as a function of $M\ddot{u}$ and the relative size of the loading, translocation and unloading zones. In this analysis, the loading zone is characterized by a constant sugar concentration $c(x) = c_0$, i.e. $\partial c/\partial x = 0$, such that equation (3.2) becomes

$$\frac{\partial^2 u}{\partial x^2} = -\frac{2L_\mathrm{p}}{r}\frac{\partial p}{\partial x} = \frac{16\eta L_\mathrm{p}}{r^3}\,u(x), \quad \text{for } 0 < x < x_1, \tag{3.3}$$

with the boundary condition $u(0) = 0$, i.e. a vanishing velocity at the beginning of the loading zone. Here, we have taken the derivative of both sides of equation (3.2*b*) in order to eliminate the pressure gradient using equation (3.2*c*). In the translocation zone, the flux $c(x)u(x)$ of sugar is conserved and equal to $c_0 u(x_1)$, where c_0 is the loading concentration and $u(x_1)$ is the velocity at the entrance of the translocation zone. This leads to an equation of the form

$$\frac{\partial^2 u}{\partial x^2} = -\frac{2L_\mathrm{p}RTc_0}{r}\frac{u(x_1)}{u^2}\frac{\partial u}{\partial x} + \frac{16\eta L_\mathrm{p}}{r^3}\,u(x), \quad \text{for } x_1 < x < x_2. \tag{3.4}$$

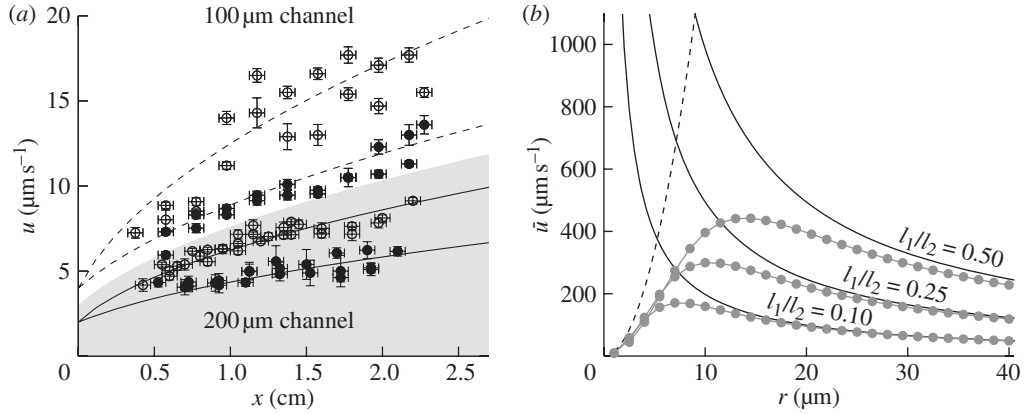

Figure 3. (*a*) Flow velocity $u(x)$ measured in 100 μm (white region) and 200 μm (grey region) deep and 200 μm wide microchannels. The dashed and solid lines are fits to equation (A 4). The sugar concentrations used are 21 mM (open circles) and 13 mM (filled circles). The horizontal error bars indicate the resolution of the microscope stage, while the vertical error bars were obtained via least squares error propagation from the velocity profile. (*b*) Numerically computed mean velocity $\bar{u}$ (dots connected by lines) as a function of radius r assuming $L_\mathrm{p} = 5 \times 10^{-14}$ m (Pa s)$^{-1}$, $l_1 = (0.1, 0.25, 0.50)$ m, $l_2 = 1$ m, $RTc_0 = 0.54$ MPa, and $\eta = 5 \times 10^{-3}$ Pa s. The solid and dashed lines show the scaling laws for u predicted by equations (3.6) and (3.7), respectively. These clearly show that $\bar{u}$ grows as r^2 for small r while it decays as $1/r$ for large r. At the intersection between the two lines given by equation (3.8) the transition between the two types of flow occurs and the velocity is at a maximum (filled circles with solid lines, numerics; solid lines, $M\ddot{u} \ll 1$; dashed lines, $M\ddot{u} \gg 1$).

The unloading zone is characterized by a linear decrease in the sugar concentration for $x_2 < x < x_3$, such that both the sugar concentration and the velocity vanish at the end of the tube, $c(x_3) = 0$ and $u(x_3) = 0$. This introduces a coefficient $\beta \equiv (l_2/c_0)(\partial c/\partial x)$, which can be determined only when we know the concentration $c(x_2)$ at the entry of the unloading zone. It can also be expressed in terms of the velocities at the entry of the translocation and unloading zones (equations (A 8*a*) and (A 8*b*)). In the unloading zone, equation (3.2) for u thus becomes

$$\frac{\partial^2 u}{\partial x^2} = -\frac{2L_\mathrm{p}RTc_0}{rl_2}\beta + \frac{16\eta L_\mathrm{p}}{r^3}u(x), \quad \text{for } x_2 < x < x_3. \tag{3.5a}$$

Our analysis of these equations is carried out in appendix A. An important simplification can be acheived by non-dimensionalization, introducing a non-dimensional length ξ (scaled by the length l_2 of the plant) and a non-dimensional velocity v scaled by the naive osmotic velocity $U = (2l_2/r)L_\mathrm{p}RTc_0$ and a non-dimensional concentration ς scaled by c_0. This gives

$$\partial_\xi^2 v = \partial_\xi \varsigma + M\ddot{u}v, \tag{3.5b}$$

where the dimensionless Münch number $M\ddot{u}$ is given by equation (3.1).

This analysis gives us a complete overview of the concentration and velocity profiles as a function of $M\ddot{u}$. Of special interest is the mean velocity $\bar{u}_2$ in the translocation zone, which sets the transit time from one end of the plant to the other. In the limit of very wide tubes, the bulk of the resistance lies in the transport of water across the membrane in the loading and unloading zone with a resistance $R_\mathrm{w} = (2\pi r l_1 L_\mathrm{p})^{-1}$. Writing the volume flux $Q = \bar{u}\pi r^2$ as $Q = \Delta p/R_\mathrm{w}$, with $\Delta p = RTc_0$, we find that the average flow velocity is $\bar{u} \approx RTc_0 L_\mathrm{p} l_1/r$. A more thorough analysis of the problem, assuming for simplicity that $l_3 = l_1$, shows that

$$\bar{u} = \left(\sqrt{3} - 1\right)\frac{RTc_0 L_\mathrm{p}}{r} l_1, \quad \text{for } M\ddot{u} \ll 1. \tag{3.6}$$

See appendix A for the full derivation, including a discussion of the case $l_3 \neq l_1$. In the opposite limit of very narrow tubes ($M\ddot{u} \gg 1$), we can argue in the following way: water moving in the system faces three barriers. First, it must pass across the membrane in the loading zone. Then, it has to move along the length of the tube before finally escaping the tube across the membrane in the unloading zone. The first and last of these three resistances are proportional to $1/r$, while the middle part scales as $1/r^4$. Thus, for very small r, the resistance in the tube $R_\mathrm{t} = 8\eta l_2(\pi r^4)^{-1}$ will dominate, giving $Q = RTc_0\pi r^4/(8\eta l_2)$, and we find an average flow velocity

$$\bar{u} = \frac{RTc_0}{8\eta l_2} r^2, \quad \text{for } M\ddot{u} \gg 1. \tag{3.7}$$

Figure 3*b* shows the numerical simulations on the full system of equations with the two expressions (3.6) and (3.7) shown as dashed and full lines, respectively. The radius (r_c) yielding the maximum velocity can be estimated as the intersection of these two curves, giving $M\ddot{u} \propto l_2/l_1$ or

$$r_\mathrm{c} = \left[8\left(\sqrt{3} - 1\right)\eta L_\mathrm{p}\right]^{1/3} l_1^{1/3} l_2^{1/3}. \tag{3.8}$$

Under the assumption that swift translocation of the phloem provides a competitive edge, it would thus be desirable for plants to have sieve tube radii close to the value r_c predicted by equation (3.8).

To explore the design constraints facing the long-distance transport in phloem, and to determine if real plants follow the scaling relation described by equation

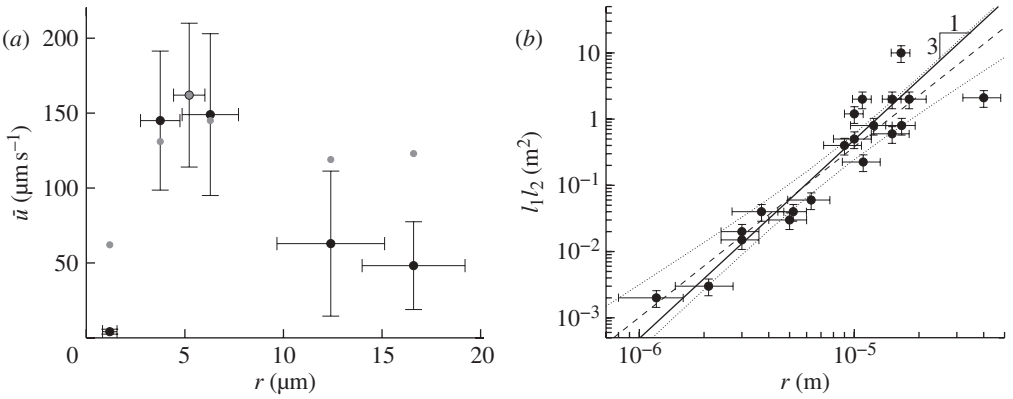

Figure 4. (*a*) *In vivo* determined phloem flow rates (black dots) in petioles (one stem) of six species plotted as a function of phloem radius as later determined on the same plant material. The velocities vary as much as 2.5 orders of magnitude, from 3 μm s^{-1} (0.01 m h^{-1}) in *T. virginiana* to 150 μm s^{-1} (0.6 m h^{-1}) in *Solanum lycopersicum*. The model predictions (grey dots) calculated from equations (3.5)–(3.7) agree well with the observed data. The error bars indicate the mean and standard errors of $N = 3$–8 measurements. (*b*) Log–log plot of $l_1 l_2$ versus measured radius r (black dots) for 20 plants of sizes ranging from $r =$ 1 μm (*T. virginiana*) to $r = 40$ μm (*Cucurbita pepo*) and $l_2 = 0.1$ m (*T. virginiana*) to $l_2 = 40$ m (*Robinia pseudoacacia*). The prediction of equation (3.8) (thick black line) with parameters $L_p = 5 \times 10^{-14}$ m (Pa s)$^{-1}$ and $\eta = 5 \times 10^{-3}$ Pa s (kinematic viscosity $= 1.85 \times 10^{-3}$, sieve plate factor $= 2.7$) is plotted along with the best fit to the plant data (dashed line, slope 2.6 ± 0.3), showing that the scaling relationship predicted by equation (3.8) falls within the 95% confidence interval (dotted lines). The error bars indicate the standard error in the radius r and lengths l_1 and l_2. See table 2 for further details on the species used.

(3.8), we examined phloem dimensions and transport velocities in real plants in petioles or stems of six species using our novel, non-invasive, dye-tracing method. Results, figure 4*a*, show that phloem velocities vary as much as a factor of 50, from 3 μm s^{-1} (0.01 m h^{-1}) in *Tradescantia virginiana* L. to 150 μm s^{-1} (0.6 m h^{-1}) in *Solanum lycopersicum* L., values consistent with the range of velocities reported using other techniques [10,12]. Comparison of velocities measured in plants with the prediction of the proposed model, figure 4*a* and equation (A 22), shows that the model reproduces the observed velocities across a wide range of species thus validating the proposed assumptions. The agreement between *in vivo* measurements (figure 4*a*) and theory derived from the analysis of osmotic-driven flow in synthetic channels (figure 3*a*) suggests that phloem flow rates are controlled by the same physical principles in plants as in biomimicking devices—at least in the low *Mü* limit, to which our microfluidic devices are so far limited—despite the anatomical complexity present in the living systems [38].

The proposed scaling law allows for the calculation of a speed-optimized radius when both loading zone and translocation length are known. Thus, we compared published data on sieve tube radii with the optimal radii calculated from equation (3.8) using leaf size as the proxy for the loading and unloading zone (l_1) and plant length as the proxy for the translocation length (l_2). The plant selection consisted of a diverse range of species, encompassed 2.5 orders of magnitude in length, and included small rosettes, grasses, vines and trees. We found good agreement between measured radii and the scaling relationships of l_1 and l_2 predicted by equation (3.8), indicating the widespread optimization of phloem dimensions for rate of translocation, figure 4*b*. Further, we found that the scaling pre-factor in equation (3.8) agrees well with the predicted optimum radii using published values of the membrane permeability L_p and the effective viscosity η. The effects of the increased flow resistance owing to the flow through the sieve plates are taken into account by multiplying the viscosity $\eta = 1.85$ mPa s of a typical plant sugar solution [10] by a so-called sieve plate factor, which typically is between 2 and 5 [6,29], for which we have assumed the value 2.7 thus arriving at the effective viscosity of 5 mPa s used in our simulations.

4. DISCUSSION

Plants are reliant on efficient and robust distribution systems made of microchannels to transport water, energy and signals over distances that range from only a few centimetres to many tens of metres. Building on the basic physical laws for osmosis, we have developed a simple, generic model for osmotically driven flow in a phloem tube with semi-permeable membranes at the wall. A single scaling law based on optimization for this theoretical translocation speed predicts phloem dimensions relative to the lengths of the loading (leaf) and unloading (root) zones and the translocation distance (stem). The existence of this optimization underscores the role of the phloem as a major informational pathway for molecular signal transduction across the plant body. It also explains why a smaller plant with large leaves (e.g. *Cucurbita*) may have larger diameter sieve tubes than found in many trees.

We have shown that our simple model for phloem translocation in plants leads to an understanding of the dependence between the speed of phloem flow and the characteristic dimensions of the plant. The assumption that plants have evolved to optimize their phloem speed then led us to a scaling relation between radius r and the characteristic lengths as $r \approx (A L_{leaf} L_{stem})^{1/3}$, where the constant A (with dimensions of length) is proportional to ηL_p, the product of

the viscosity of the flow and the permeability of the membrane, a prediction which is supported by field-data from plants. It should be noted that the optimization over the radius is done while fixing the lengths L_{leaf} and L_{stem} of the plant. The corresponding optimal velocity can approximately be obtained by inserting $r = r_{\mathrm{c}}$, given by equation (3.8), into equation (3.6) or (3.7), giving

$$u_{\mathrm{opt}} = aRTc_0\, L_{\mathrm{p}}^{2/3}\boldsymbol{\eta}^{-1/3}L_{\mathrm{leaf}}^{2/3}L_{\mathrm{stem}}^{-1/3},$$

where a is a numerical constant. Thus an increase of the leaf size (with fixed stem size) will lead to an increase in the velocity, while an increase of the stem size (with fixed leaf size) will lead to a decrease. We thus assume that these external length scales are set by other biological constraints such as the cost of building, supporting and maintaining photosynthetic surfaces.

The challenges faced by the phloem in moving photo-assimilates over long distances led to the suggestion that the axial pathway is compartmentalized into 'relays', such that solutes are actively reloaded at discrete points [39]. Relays increase the rate of phloem transport, but require additional inputs of energy. Although no empirical evidence exists for relays, their potential contribution to phloem transport has been widely considered [32,40]. Our analysis, which uses the length of the entire plant as proxy for l_2, is not consistent with the presence of relays, suggesting that axial compartmentalization is not a necessary design feature for efficient phloem transport.

Plants, which span tens of metres and proliferate in hundreds of cubic metres of soil and air, experience diverse and often rapid fluctuations in environmental conditions. To respond to such environmental heterogeneity requires the rapid distribution of both energy and information in the form of chemical signals to enhance plant productivity and competitiveness. The phloem provides uninterrupted coupling between most distal parts of all plants and links plants' multi-branched dendritic structure into a single functional microfluidic system [41]. Concordance between our theoretical model, studies of osmotically driven flow in synthetic phloem, and measurements of flow and geometric properties made on real plants gives confidence in the Münch theory of phloem flow and suggests that plants are optimized for rapid translocation of sugar, thereby gaining a competitive edge in terms of their ability to respond rapidly to environmental stimuli. Our analysis provides a general scaling law for phloem dimensions that maximizes translocation velocity, suggesting that evolutionary selection on the efficacy of signal transduction has shaped the structure and function of this supracellular transport pathway.

We thank Howard Stone and Matthew Thompson for comments on the manuscript. This work was supported by the Danish National Research Foundation (grant no. 74), the Andrew W. Mellon Foundation and the Materials Research Science and Engineering Centre at Harvard University.

APPENDIX A

Analysis of the Münch equation (3.2*b*) is facilitated by making it dimensionless using the following rescaling of length, velocity and concentration:

$$x = \boldsymbol{\xi}\, l_2, \quad u = Uv = \left(\frac{2l_2}{r}L_{\mathrm{p}}RTc_0\right)v \quad \text{and} \quad c = \boldsymbol{\varsigma}\, c_0, \tag{A 1}$$

whereby the non-dimensional Münch equation becomes

$$\partial_{\xi}^2 v = \partial_{\xi}\boldsymbol{\varsigma} + M\ddot{u}v, \quad \text{for } 0 < \boldsymbol{\xi} < \xi_3. \tag{A 2}$$

The three zones are the loading zone ($0 < \boldsymbol{\xi} < \xi_1$) of length $\boldsymbol{\lambda}_1 = \boldsymbol{\alpha} = l_1/l_2$, the translocation zone ($\xi_1 < \boldsymbol{\xi} < \xi_2$) of length $\boldsymbol{\lambda}_2 = 1$, and the unloading zone ($\xi_2 < \boldsymbol{\xi} < \xi_3$) of length $\boldsymbol{\lambda}_3 = \boldsymbol{\alpha} = l_1/l_2$.

The zero-end-pressure phloem transport model. In the literature (see [6] and references therein), the correct choice of boundary conditions remains unclear, primarily due to lack of knowledge of the exact physiological processes in the loading and unloading zones. This has led to a large class of models all based on equation (A 2), but with widely different boundary conditions. The method applied by most workers has been to either ignore the loading and unloading zones by setting simple conditions at the edges of the translocation zone or to use specific loading and unloading functions. A special case of these models examined by Hölttä *et al.* [40] is to set the pressure at the end of the translocation zone to a fixed value, say $p = 0$. In the microfluidic experiments, we have tested this limit experimentally, and we now consider the solution to equation (A 2) under these conditions.

In the microfluidic channel zone, here defined as $0 < \boldsymbol{\xi} < 1$, equation (A 2) becomes

$$\frac{\partial^2 v}{\partial \boldsymbol{\xi}^2} = -\frac{v_0}{v^2}\frac{\partial v}{\partial \boldsymbol{\xi}} + M\ddot{u}v, \quad \text{for } 0 < \boldsymbol{\xi} < 1, \tag{A 3a}$$

with the boundary conditions

$$v(0) = v_0 \tag{A 3b}$$

and

$$p(1) = 0. \tag{A 3c}$$

In the experiments $M\ddot{u}$ is very small, so combining $M\ddot{u} = 0$ with equation (A 3*b*) yields

$$v(\boldsymbol{\xi}) = v_0^{1/2}(v_0 + 2\boldsymbol{\xi})^{1/2}, \tag{A 4}$$

in good agreement with the experimetal results (figure 3*a*).

The loading/unloading phloem transport model. We now return to the more general three-zone model of the phloem translocation pathway (figure 1). We assume that the loading and unloading zones are of equal size ($l_1 = l_3$), that the concentration c is constant and equal to c_0 in the loading zone and that the concentration profile is linearly decreasing in the unloading zone. The quantity

we wish to calculate is the mean flow velocity $\bar{u}$ in the translocation zone as a function of $M\ddot{u}$ and $\alpha = l_1/l_2$. The boundary conditions on the velocity v is that it is zero at the boundaries,

$$v(0) = v(\xi_3) = 0. \tag{A 5}$$

In the loading zone, the concentration ς is assumed to be constant and equal to unity,

$$\varsigma_1(\xi) = 1, \quad \text{for } 0 < \xi < \xi_1. \tag{A 6}$$

In the translocation zone, we have sugar flux conservation,

$$v_2(\xi)\varsigma_2(\xi) = \varsigma_3(\xi_2)v_3(\xi_2) = v_2(\xi_1), \quad \text{for } \xi_1 < \xi < \xi_2. \tag{A 7}$$

In the unloading zone, we assume that the concentration profile is linear and of the form

$$\varsigma_3(\xi) = -\beta(\xi - \xi_3), \quad \text{for } \xi_2 < \xi < \xi_3, \tag{A 8a}$$

where β is determined from sugar conservation (A 6) and (A 7) in the translocation zone,

$$\beta = \frac{v_2(\xi_1)}{v_2(\xi_2)(\xi_3 - \xi_2)}. \tag{A 8b}$$

The equations of motion are

$$\partial_\xi^2 v_1 = M\ddot{u}v_1, \quad \text{for } 0 < \xi < \xi_1, \tag{A 9a}$$

$$\partial_\xi^2 v_2 = -\frac{v_1(\xi_1)}{v_2^2}\partial_\xi v_2 + M\ddot{u}v_2, \quad \text{for } \xi_1 < \xi < \xi_2, \tag{A 9b}$$

and $$\partial_\xi^2 v_3 = -\beta + M\ddot{u}v_3, \quad \text{for } \xi_2 < \xi < \xi_3. \tag{A 9c}$$

Here, the indices on v indicate the domain to which it belongs. These equations cannot be solved analytically for arbitrary values of $M\ddot{u}$ and α; however, analytical solutions can be found in the limits $M\ddot{u} \ll 1$ and $M\ddot{u} \gg 1$. These analytical solutions allow us to calculate the mean flow velocity $\bar{u}$ as a function of the parameters in the problem. Keeping, say, l_1 and l_2 fixed while varying the tube radius r, we find that the analytical solutions allow us to determine the point in the parameter space where the average translocation speed $\bar{u}$ is at a maximum.

Solution for $M\ddot{u} \ll 1$. In this limit, the equations of motion (A 9*a*)–(A 9*c*) are

$$\partial_\xi^2 v_1 = 0, \quad \text{for } 0 < \xi < \xi_1, \tag{A 10a}$$

$$\partial_\xi^2 v_2 = -\frac{v_1(\xi_1)}{v_2^2}\partial_\xi v_2, \quad \text{for } \xi_1 < \xi < \xi_2, \tag{A 10b}$$

and $$\partial_\xi^2 v_3 = -\beta, \quad \text{for } \xi_2 < \xi < \xi_3, \tag{A 10c}$$

with the boundary conditions $v_1(0) = 0$ and $v_3(\xi_3) = 0$. The solutions can be written as

$$v_1(\xi) = C_1\xi + C_2, \tag{A 11a}$$

$$\xi(v_2) = \frac{v_1(\xi_1)}{C_5}\left[\frac{v_2}{v_1(\xi_1)} - \frac{1}{C_5}\log\left(\frac{1 + (C_5 v_2/v_1(\xi_1))}{1 + C_5}\right)\right] + C_6 \tag{A 11b}$$

and $$v_3(\xi) = -\frac{1}{2}\frac{v_2(\xi_1)}{v_2(\xi_2)}\frac{1}{(\xi_3 - \xi_2)}(\xi - \xi_3)^2 + C_3(\xi - \xi_3) + C_4. \tag{A 11c}$$

By demanding that the velocity and its derivative should be continous at $\xi = \xi_1$ and $\xi = \xi_2$, and that $\alpha \ll 1$, we find the six C coefficients above to be

$$(C_1, C_2, C_3, C_4, C_5, C_6) = \Big(2 - \sqrt{3},\ 0,\ 1 - \sqrt{3},\ 0,\ 1 - \sqrt{3},\ \lambda_1\lfloor 1 + \sqrt{3}\rfloor/2\Big). \tag{A 12}$$

The mean velocity $\bar{v}$ is then

$$\bar{v} = \frac{\sqrt{3} - 1}{2}\lambda_1 - \frac{9 - 5\sqrt{3}}{8}\lambda_1^2 \approx 0.366\,\lambda_1 - 0.043\,\lambda_1^2, \tag{A 13}$$

which in dimensional units for small values of λ_1, i.e. $l_1 \ll l_2$, becomes equation (3.6).

Solution for $M\ddot{u} \gg 1$. The equations of motion are

$$\partial_\xi^2 v_1 = M\ddot{u}v_1, \quad \text{for } 0 < \xi < \xi_1, \tag{A 14a}$$

$$\partial_\xi^2 v_2 = -\frac{v_1(\xi_1)}{v_2^2}\partial_\xi v_2 + M\ddot{u}v_2, \quad \text{for } \xi_1 < \xi < \xi_2 \tag{A 14b}$$

and $$\partial_\xi^2 v_3 = -\beta + M\ddot{u}v_3, \quad \text{for } \xi_2 < \xi < \xi_3, \tag{A 14c}$$

with the boundary conditions $v_1(0) = 0$ and $v_1(\xi_3) = 0$. In zones 1 and 3, the solutions are

$$v_1(\xi) = A_1 \sinh\sqrt{M\ddot{u}}\xi + A_2 \cosh\sqrt{M\ddot{u}}\xi, \quad \text{for } 0 < \xi < \xi_1 \tag{A 15a}$$

and

$$v_3(\xi) = A_3 \sinh\sqrt{M\ddot{u}}(\xi - \xi_2) + A_4 \cosh\sqrt{M\ddot{u}}(\xi - \xi_2) + \frac{\beta}{M\ddot{u}}, \quad \text{for } \xi_2 < \xi < \xi_3. \tag{A 15b}$$

Here, $A_2 = 0$ because of the boundary condition at $\xi = 0$, while A_3 and A_4 are determined by the continuity condition on v and $\partial_\xi v$ at $\xi = \xi_2$:

$$A_3 = \frac{1}{\sqrt{M\ddot{u}}}\partial_\xi v_2(\xi_2) \tag{A 15c}$$

and

$$A_4 = v_2(\xi_2) - \frac{\beta}{M\ddot{u}}. \tag{A 15d}$$

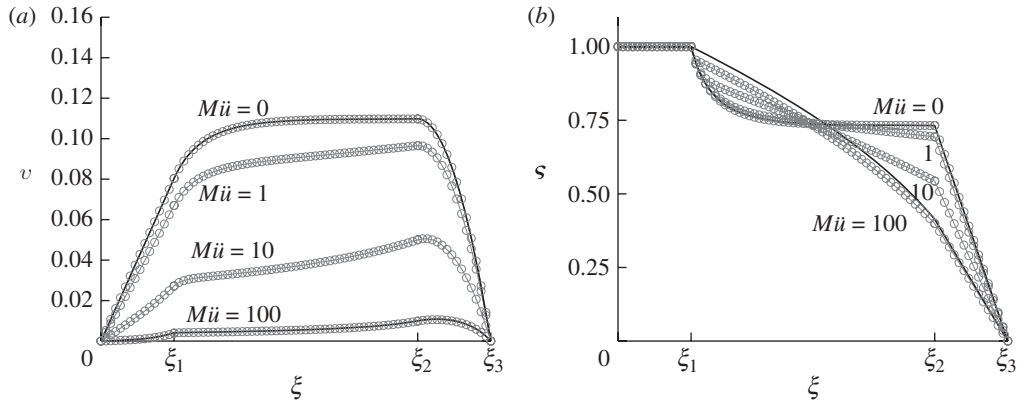

Figure 5. Comparison between analytical and numerical solutions of the non-dimensional phloem flow problem. (*a*) Numerically computed velocity v (circles) as a function of position ξ for $M\ddot{u} = 0$, 1, 10, 100, $\xi_1 = 0.3$, $\xi_2 = 1.3$ and $\xi_3 = 1.6$. The analytical solutions for the velocity (solid lines) given in equations (A 11*a–c*), (A 15*a*,*b*) and (A 18) are shown for comparison. (*b*) Numerically computed concentration ς (circles) as a function of position ξ for the same parameters as in (*a*). The analytical solutions for the concentration (solid lines) were found using the solutions for v given in equations (A 11*a–c*), (A 15*a*,*b*) and (A 18) and the conditions given in equations (A 6), (A 7) and (A 8*a*,*b*). Open circles, numerics; solid lines, analytics.

Table 2. Plant data used in figure 4 for phloem type P (primary = 1, secondary = 2). Sieve lumen radius r, translocation zone length l_2 (plant length), loading zone length l_1 (leaf size) and measured flow velocity are given with corresponding standard deviations. The Münch number $M\ddot{u}$ and the ratio l_1/l_2 were calculated using $L_p = 5 \times 10^{-14}\,\mathrm{m\,s^{-1}\,Pa^{-1}}$, $\eta = 5 \times 10^{-3}$ Pa s. Estimates of l_1 and l_2 follow general knowledge of plants available at online databases (USDA plant database) and visits to the Harvard University Herbaria. References are given in square brackets.

species	habit	P	r (μm)	Δr (μm)	l_2 (m)	Δl_2 (m)	l_1 (m)	Δl_1 (m)	u (μm s^{-1})	Δu (μm s^{-1})	$M\ddot{u}$	l_1/l_2
Beta vulgaris	herbaceous dicot	1	5.0 [42–44]	1.0	0.3	0.06	0.10	0.02			2.88	0.33
Yucca flaccida	woody monocot	1	10.0 [44]	2.0	1.0	0.2	0.5	0.1			4.00	0.50
Sabal palmetto	tree monocot	1	16.5 [44]	1.7	20	4	0.5	0.1			35.6	0.025
Tilia americana	tree dicot	2	15.0 [44]	1.5	20	4	0.10	0.02			474	0.0050
Robinia pseudoacacia	tree dicot	2	10.0 [44]	1.0	40	8	0.030	0.006			6400	0.00075
Vitis vinifera	vine	2	18.0 [44]	4.0	20	4	0.10	0.02			274	0.0050
Gossypium bardadense	herbaceous dicot	1	11.0 [44]	2.2	1.5	0.3	0.15	0.03			6.76	0.10
Pinus strobus	tree conifer	2	10.9 [45]	1.0	20	4	0.10	0.02			1240	0.0050
Festuca arundinacea	herbaceous monocot	1	3.0 [46]	0.6	0.30	0.06	0.05	0.01			13.3	0.17
Cucurbita pepo	creeper dicot	2	40.0 [47]	8.0	7.0	1.4	0.30	0.06			3.06	0.043
Glycine max	herbaceous dicot	1	3.7[a]	1.0	0.40	0.08	0.10	0.02	145	46	12.6	0.25
Tradescantia virginiana	herbaceous monocot	1	1.2[a]	0.4	0.10	0.02	0.020	0.004	4.13	1.64	23.1	0.20
Cucumis sativus	creeper dicot	1	6.3[a]	1.4	0.60	0.12	0.10	0.02	149	54	5.76	0.17
Cucurbita maxima	creeper dicot	1	12.3[a]	2.7	4.0	0.8	0.20	0.04	62.9	48.4	34.4	0.050
Cucurbita maxima	creeper dicot	2	16.6[a]	2.6	4.0	0.8	0.20	0.04	48.2	29.3	14.0	0.050
Solanum lycopersicum	herbaceous dicot	1	5.2[a]	0.8	0.40	0.08	0.10	0.02	162	48	4.55	0.25
Anacyclus purethrum	herbaceous dicot	1	2.1 [10]	0.6	0.30	0.06	0.010	0.002			38.9	0.033
Ecbalium elaterium	creeper dicot	1	15.0 [10]	3.0	3.0	0.6	0.20	0.04			10.7	0.067
Eragostis plana	herbaceous monocot	1	3.0 [48]	0.6	0.2	0.04	0.10	0.02			5.93	0.5
Heracleum mantegazzianum	herbaceous dicot	1	9.0 [49]	1.8	2.0	0.4	0.20	0.04			21.9	0.1

[a]Refers to our own measurements.

In the translocation zone, we shall solve the equation

$$\partial_\xi^2 v_2 = -\frac{v_1(\xi_1)}{v_2^2}\partial_\xi v_2 + M\ddot{u}v_2, \quad \text{for } \xi_1 < \xi < \xi_2, \tag{A 16}$$

by assuming that v_2 can be written as $v_2 = v'_2/M\ddot{u}$, where v'_2 is of the order of unity. Inserting this, and keeping only terms of order $M\ddot{u}$ and $M\ddot{u}^2$, we get that

$$M\ddot{u}v_1(\xi_1)\partial_\xi v'_2 = v_2^{3\prime}. \tag{A 17}$$

Since we must have that $v_2(\xi_1) = v_1(\xi_1)$, we get that

$$v_2(\xi) = \frac{v_1(\xi_1)}{\sqrt{1 - 2M\ddot{u}v_1(\xi_1)(\xi - \xi_1)}}, \quad \text{for } \xi_1 < \xi < \xi_2. \tag{A 18}$$

Note that this solution does not fulfil the condition $\partial_\xi v_2(\xi_1) = \partial_\xi v_1(\xi_1)$. This is due to the fact that we have ignored the term $\partial_\xi^2 v_2$. However, this turns out to play very little role when comparing the analytical solution with the numerical solution of the full problem. Using the continuity conditions at $\xi = \xi_1$ and $\xi = \xi_2$, the mean translocation velocity $\bar{v}$ in the translocation zone is found to be

$$\bar{v} = \frac{1}{M\ddot{u}}, \tag{A 19}$$

which in dimensional units becomes equation (3.7). Representative examples of numerical solutions for the dimensionless velocity and concentration fields together with the analytical solutions for small and large $M\ddot{u}$ are shown in figure 5.

Different sizes of the loading and unloading zone. If $l_1 \neq l_3$, we find that for $M\ddot{u} \gg 1$ the solution (A 19) remains unchanged, while for $M\ddot{u} \ll 1$ the mean velocity instead of equation (A 13) now is given by

$$\bar{v} = \frac{1}{2}\lambda_1\left(\sqrt{1 + 2\chi} - 1\right), \tag{A 20}$$

where $\chi = \lambda_3/\lambda_1$. Thus the scaling relations are not significantly affected as long as χ is of the order of unity.

Optimal radius of the phloem tubes. To maximize the flow velocity, a plant would presumably operate near the maximum in the u–r diagram shown in figure 3*b*. Equating the two expressions (3.6) and (3.7) for $\bar{u}$ in the limits $M\ddot{u} \ll 1$ and $M\ddot{u} \gg 1$ gives the following estimate for the optimal radius r_c:

$$r_c^3 = 8(\sqrt{3} - 1)L_p\eta l_1 l_2. \tag{A 21}$$

Phloem translocation velocity. Figure 4*a* shows the velocities $\bar{u}$ measured experimentally (black circles) using the method described in figure 2. To compare our model with the experimental data, the non-dimensional mean velocity $\bar{v}$ depending on $M\ddot{u}$ and α was first calculated numerically from equations (A 5)–(A 9*c*) using the data for r and l_2 shown in table 2. Then, the dimensional mean velocity $\bar{u}$ was found from

$$\bar{u}(M\ddot{u}, \alpha) = \frac{2l_2}{r}L_p RTc_0\bar{v}(M\ddot{u}, \alpha), \tag{A 22}$$

with $L_p = 5 \times 10^{-14}\,\mathrm{m\,(Pa\,s)^{-1}}$ chosen as the representative value and $RTc_0 = 0.54$ MPa chosen to fit the model to the experimental value for *S. lycopersicum*. These predicted values for $\bar{u}$ (grey circles) are also plotted in figure 3*b* showing good agreement between theory and experiment.

REFERENCES

1 Holbrook, N. & Zwieniecki, M. 2008 Transporting water to the tops of trees. *Phys. Today* **61**, 76–77. (doi:10.1063/1.2835167)

2 Tyree, M. T. & Zimmermann, M. H. 2002 *Xylem structure and the ascent of sap*, 2nd edn. Berlin, Germany: Springer.

3 Knoblauch, M. & Peters, W. S. 2010 Münch, morphology, microfluidics—our structural problem with the phloem. *Plant Cell Environ.* **33**, 1439–1452. (doi:10.1111/j.1365-3040.2010.02177.x)

4 van Bel, A. J. E. & Hafke, J. B. 2005 Physiochemical determinants of phloem transport. In *Vascular transport in plants* (eds N. M. Holbrook & M. A. Zwieniecki), pp. 19–44. San Diego, CA: Elsevier Academic Press.

5 Pickard, W. F. & Abraham-Shrauner, B. 2009 A 'simplest' steady-state Münch-like model of phloem translocation, with source and pathway and sink. *Funct. Plant Biol.* **36**, 629–644. (doi:10.1071/FP08278)

6 Thompson, M. V. & Holbrook, N. M. 2003 Application of a single-solute non-steady-state phloem model in the study of long-distance assimilate transport. *J. Theor. Biol.* **220**, 419–455. (doi:10.1006/jtbi.2003.3115)

7 Lough, T. J. & Lucas, W. J. 2006 Integrative plant biology: role of phloem long-distance macromolecular trafficking. *Ann. Rev. Plant Biol.* **57**, 203–232. (doi:10.1146/annurev.arplant.56.032604.144145)

8 Turgeon, R. & Wolf, S. 2009 Phloem transport: cellular pathways and molecular trafficking. *Ann. Rev. Plant Biol.* **60**, 207–221. (doi:10.1146/annurev/arplant.043008.092045)

9 Mencuccini, M. & Hölttä, T. 2010 The significance of phloem transport for the speed with which canopy photosynthesis and belowground respiration are linked. *New Phytol.* **185**, 189–203. (doi:10.1111/j/1469-8137.2009.03050.x)

10 Canny, M. J. 1973 *Phloem translocation*. Cambridge, UK: Cambridge University Press.

11 Milburn, J. A. 1975 Pressure flow. In *Transport in plants I. Phloem transport* (eds M. H. Zimmermann & J. A. Milburn), pp. 328–353. Berlin, Germany: Springer.

12 Windt, C. W., Vergeldt, F. J., de Jager, P. A. & van As, H. 2006 MRI of long-distance water transport: a comparison of the phloem and xylem flow characteristics and dynamics in poplar, castor bean, tomato and tobacco. *Plant Cell Environ.* **29**, 1715–1729. (doi:10.1111/j1365.3040.2006.01544.x)

13 Sperry, J. S., Meinzer, F. C. & McCulloch, K. A. 2008 Safety and efficiency conflicts in hydraulic architecture: scaling from tissues to trees. *Plant Cell Environ.* **31**, 632–645. (doi:10.1111/j/1365-3040.2007.01765.x)

14 Knoblauch, M., Noll, G. A., Müller, T., Prüfer, D., Schneider-Hüther, I., Scharner, D., van Bel, A. J. E. & Peters, W. S. 2003 ATP-independent contractile proteins from plants. *Nat. Mater.* **2**, 600–603. (doi:10.1038/nmat960)

15 Sjolund, R. D. 1997 The phloem sieve element: a river runs through it. *Plant Cell* **9**, 1137–1146. (doi:10.1105/tpc.9.7.1137)

16 Fisher, D. B. 2000 Long-distance transport. In *Biochemistry and molecular biology of plants* (eds B. B. Buchanan,

W. GruissemR. J. Jones), pp. 730–784. Rockville, MD: American Society of Plant Physiologists.
17 Wheeler, T. D. & Stroock, A. D. 2008 The transpiration of water at negative pressures in a synthetic tree. *Nature* **455**, 208–212. (doi:10.1038/nature07226)
18 Noblin, X., Mahadevan, L., Coomaraswamy, I. A., Weitz, D. A., Holbrook, N. M. & Zwieniecki, M. A. 2008 Optimal vein density in artificial and real leaves. *Proc. Natl Acad. Sci. USA* **105**, 9140–9144. (doi:10.1073/pnas.0709194105)
19 Jensen, K. H., Lee, J., Bohr, T. & Bruus, H. 2009 Osmotically driven flows in microchannels separated by a semipermeable membrane. *Lab Chip* **9**, 2093–2099. (doi:10.1039/b818937d)
20 Münch, E. 1943 Durchlässigkeit der siebröhren fur druckströmungen. *Flora* (*Jena, 1818–1965*) **136**, 223–262.
21 Christy, A. L. & Ferrier, J. M. 1973 A mathematical treatment of Münch's pressure-flow hypothesis of phloem translocation. *Plant Physiol.* **52**, 531–538.
22 Goeschl, J. D., Magnuson, C. E., DeMichele, D. W. & Sharpe, P. J. H. 1976 Concentration-dependent unloading as a necessary assumption for a closed form mathematical model of osmotically driven pressure flow in phloem. *Plant Physiol.* **58**, 556–562.
23 Henton, S. M., Greaves, A. J., Piller, G. J. & Minchin, P. E. H. 2002 Revisiting the Münch pressure-flow hypothesis long-distance transport of carbohydrates: modelling the dynamics of solute transport inside a semipermeable tube. *J. Exp. Bot.* **53**, 1411–1419. (doi:10.1093/jexbot/53.373.1411)
24 Smith, K. C., Magnuson, C. E., Goeschl, J. D. & DeMichele, D. W. 1980 A time-dependent mathematical expression of the Münch hypothesis of phloem transport. *J. Theor. Biol.* **86**, 493–505. (doi:10.1016/0022-5193(80)90348-3)
25 van Bel, A., Ehlers, K. & Knoblauch, M. 2002 Sieve elements caught in the act. *Trends Plant Sci.* **7**, 126–132. (doi:10.1016/S1360-1385(01)02225-7)
26 Canny, M. 1975 Mass transfer. In *Transport in plants I. Phloem transport* (eds M. H. Zimmermann & J. A. Milburn), pp. 139–153. Berlin, Germany: Springer.
27 Minchin, P. E. H. & Thorpe, M. R. 2003 Using the short-lived isotope ^{11}C in mechanistic studies of photosynthate transport. *Funct. Plant Biol.* **30**, 831–841. (doi:10.1071/FP03008)
28 Knoblauch, M. & van Bel, A. J. E. 1998 Sieve tubes in action. *Plant Cell* **10**, 35–50. (doi:10.1105/tpc.10.1.35)
29 Mullendore, D. L., Windt, C. W., Van As, H. & Knoblauch, M. 2010 Sieve tube geometry in relation to phloem flow. *Plant Cell* **22**, 579–593. (doi:10.1105/tpc.109.070094)
30 Bao, J.-B. & Harrison, D. J. 2006 Measurement of flow in microfluidic networks with micrometer-sized flow restrictors. *AIChE J.* **52**, 75–85. (doi:10.1002/aic.10612)
31 Schrum, K. F., Lancaster LII, J. M., Johnston, S. E. & Gilman, S. D. 2000 Monitoring electroosmotic flow by periodic photobleaching of a dilute, neutral fluorophore. *Anal. Chem.* **72**, 4317–4321. (doi:10.1021/ac0005114)
32 Thompson, M. 2006 Phloem: the long and the short of it. *Trends Plant Sci.* **11**, 26–32. (doi:10.1016/j.tplants.2005.11.009)
33 Jensen, K. H., Rio, E., Hansen, R., Clanet, C. & Bohr, T. 2009 Osmotically driven pipe flows and their relation to sugar transport in plants. *J. Fluid Mech.* **636**, 371–396. (doi:10.1017/S002211200900799X)
34 Aldis, G. K. 1988 The unstirred layer during osmotic flow into a tubule. *Bull. Math. Biol.* **50**, 531–545. (doi:10.1016/S0092-8240(88)80007-7)
35 Phillips, R. J. & Dungan, S. R. 1993 Asymptotic analysis of flow in sieve tubes with semi-permeable walls. *J. Theor. Biol.* **162**, 465–485. (doi:10.1006/jtbi.1993.1100)
36 Eschrich, W., Evert, R. F. & Young, J. H. 1972 Solution flow in tubular semipermeable membranes. *Planta* **107**, 279–300. (doi:10.1007/BF00386391)
37 Lang, A. 1973 A working model of a sieve tube. *J. Exp. Bot.* **24**, 896–904. (doi:10.1093/jxb/24.5.896)
38 Esau, K. 1965 *Plant anatomy*. New York, NY: John Wiley & Sons, Inc.
39 Lang, A. 1979 A relay mechanism for phloem translocation. *Ann. Bot.* **44**, 141–145. (doi:0305-7364/79/080141+05S02.00/0)
40 Hölttä, T., Mencuccini, M. & Nikinmaa, E. 2009 Linking phloem function to structure: analysis with a coupled xylem–phloem transport model. *J. Theor. Biol.* **259**, 325–337. (doi:10.1016/j.jtbi.2009.03.039)
41 van Bel, A. J. E. 2003 The phloem, a miracle of ingenuity. *Plant Cell Environ.* **26**, 125–149. (doi:10.1046/j.1365.3040.2003.00963.x)
42 Geiger, D. & Cataldo, D. 1969 Leaf structure and translocation in sugar beet. *Plant Physiol.* **44**, 45–54. (doi:10.1104/pp.44.1.45)
43 Sokolova, S. 1968 Fine structure of petiole phloem cells of *Beta vulgaris* L. *Plant Physiol.* (*Russian*) **15**, 757–763.
44 Tyree, M. T., Christy, A. L. & Ferrier, J. M. 1974 A simpler iterative steady state solution of Münch pressure-flow systems applied to long and short translocation paths. *Plant Physiol.* **54**, 589–600. (doi:10.1104/pp.54.4.589)
45 Murmanis, L. & Evert, R. 1966 Some aspects of sieve cell ultrastructure in *Pinus strobus*. *Am. J. Bot.* **53**, 1065–1078. (doi:10.2307/2440687)
46 Sheehy, J., Mitchell, P., Durnand, J., Gastal, F. & Woodward, F. 1995 Calculation of translocation coefficients from phloem anatomy for use in crop models. *Ann. Bot.* **76**, 263–269. (doi:10.1006/anbo.1995.1095)
47 Crafts, A. & Lorenz, O. 1944 Fruit growth and food transport in cucurbits. *Plant Physiol.* **19**, 131–138. (doi:10.1104/pp.19.1.131)
48 Botha, C. 2005 Interaction of phloem and xylem during phloem loading: functional sympalsmic roles for thin- and thick-walled sieve tubes in monocotyledons. In *Vascular transport in plants* (eds N. M. Holbrook & M. A. Zwieniecki), pp. 115–130. San Diego, CA: Elsevier Academic Press.
49 Fensom, D. 1975 Work with isolated phloem strands. In *Transport in plants I: phloem transport* (eds M. H. Zimmermann & J. A. Milburn), pp. 223–244. Berlin, Germany: Springer.